Contents lists available at ScienceDirect

Transactions of Nonferrous Metals Society of China

36(2026) 259−272

www.tnmsc.cn

Low-temperature bonding of W90 tungsten heavy alloy using Sn−2Al filler metal by ultrasonic-assisted coating technology

Xiao-guo SONG[a,b], Xu-dong ZHANG[a,b], Wei FU[a,b,*], Xiao-yu TIAN[c], Guang-dong WU[c], Sheng-peng HU[a,b]

[a] State Key Laboratory of Precision Welding & Joining of Materials and Structures, Harbin Institute of Technology, Harbin 150001, China;

[b] Shandong Provincial Key Laboratory of Special Welding Technology, Harbin Institute of Technology, Weihai 264209, China;

[c] Beijing Institute of Control Engineering, Beijing 100190, China

Abstract: The Sn−2Al filler metal was utilized to bond W90 tungsten heavy alloys by the ultrasonic-assisted coating technology in atmospheric environment at 250 °C. The effects of ultrasonic power and ultrasonic time on microstructure and interfacial strength of Sn−2Al/W90 interface were investigated. The ultrasound improved the wettability of Sn−2Al filler metal on W90 surface. As the ultrasonic power increased and ultrasonic time increased, the size of Al phase in seam decreased. The maximum value of Sn−2Al/W90 interfacial strength reached 30.1 MPa. Based on the acoustic pressure simulation and bubble dynamics, the intensity of cavitation effect was proportional to ultrasonic power. The generated high temperature and high pressure by cavitation effect reached 83799.6 K and 1.26×10^{14} Pa, respectively.

Keywords: W−Ni−Fe alloy; Sn−Al filler metal; ultrasonic-assisted coating technology; acoustic pressure; cavitation; bubble dynamics

1 Introduction

In order to meet the rapidly growing demand for performance and reliability as well as environmental protection and energy conservation, many researchers have developed a variety of multi-material combinations to fully utilize the properties of each material combinations [1,2]. Tungsten heavy alloy is a dual-phase metallic composites consisting of spherical W grains surrounded by a metallic binder phase such as Fe, and Ni. It is an important candidate of radiation shielding material due to its higher linear attenuation coefficient and smaller half-value layer [3,4]. However, the application of tungsten heavy alloy is limited due to its high density and high raw-material cost, especially in the aerospace field. The reliable welding between tungsten heavy alloys and lightweight materials, such as Al and Mg, is commonly involved to satisfy the requirements for lightweight [5].

Currently, reliable joining of tungsten heavy alloy is usually achieved by high temperature brazing and diffusion, for which long dwelling time and elevated process temperatures of 800 to 1340 °C are generally required [6,7]. However, the above methods are clearly unsuitable for joining tungsten heavy alloy to Al and Mg alloys. The high-temperature bonding and significant differences in coefficient of thermal expansion (CTE) between them can easily lead to large residual thermal stresses, resulting into welding manufacturing defects.

Corresponding author: *Wei FU, Tel/Fax: +86-631-5678454, E-mail: wei.fu@hit.edu.cn

https://doi.org/10.1016/S1003-6326(25)66962-7

Received 23 April 2024; accepted 27 December 2024

Ultrasonic-assisted soldering is an effective method for dissimilar materials to substantially reduce the process temperature and thus avoid the generation of thermal cracking [8,9]. During the ultrasonic-assisted soldering, the ultrasonic head generates high-frequency oscillations in liquid filler metal, resulting into the nucleation, growth, oscillation, and collapse of cavitation bubble [10,11]. The collapse of cavitation bubble gives rise to various unique phenomena, such as locally high temperature, high pressure, micro-jet and shock wave [12,13], which creates an extremely non-equilibrium physicochemical environment to meet the reaction condition [14,15]. DONG et al [16,17] successfully performed the reliable bonding between ZrO_2 ceramic and Al alloy using Sn−Al filler metal by ultrasonic-assisted soldering. The amorphous Al_2O_3 layer was formed at the interface between ZrO_2 ceramic and Sn−Al filler metal under the action of ultrasound. Besides, the ultrasonic-assisted coating technology has been successfully applied to the low-temperature bonding of ceramic and metal [18]. The technology can avoid the breakage of the base materials, compared with ultrasonic directly applying on the base material surface.

Currently, the joining of tungsten heavy alloy is primarily conducted at high temperature, and there are limited proposals for low-temperature bonding technology of tungsten heavy alloy. In this work, the ultrasonic-assisted coating technology was first proposed for the low-temperature bonding of W90 tungsten heavy alloy using Sn−2Al filler metal. The ultrasonic-assisted coating technology was divided into two steps. First, Sn−2Al coating was prepared on the W90 surface under the action of ultrasound, and then the coatings were assembled face-to-face and bonded at 250 °C. The effects of ultrasonic power and ultrasonic time on the microstructures and interfacial strength of Sn−2Al/W90 interface were investigated. Besides, the cavitation characteristics and variation process were studied and then correlated by acoustic pressure simulation.

2 Experimental

2.1 Materials and processing technique

W90 tungsten heavy alloy (W90, Qinghe Dingyuan Metal Product Co., Xingtai, China) and Sn−2wt.%Al alloy prepared by arc melting were selected as substrate and filler metal in this work, respectively. The pure tin (99.98 wt.%) and pure aluminum (99.95 wt.%) blocks were provided by Zhejiang Metallurgical Research Institute, Hangzhou, China. The W90 consisted of W particle and (Ni,Fe) matrix phase and Sn−2Al alloy was composed of the matrix phase of Sn and Al phase [19]. The schematic diagram of ultrasonic-assisted coating process is shown in Fig. 1(a), in which both the assembled W90 and the Sn−2Al filler metal were heated to a set temperature, and then the ultrasonic horn was pressed on the faying surface of liquid Sn−2Al filler metal, where the process temperature and ultrasonic frequency were 250 °C and 20 kHz, respectively. The distance between the

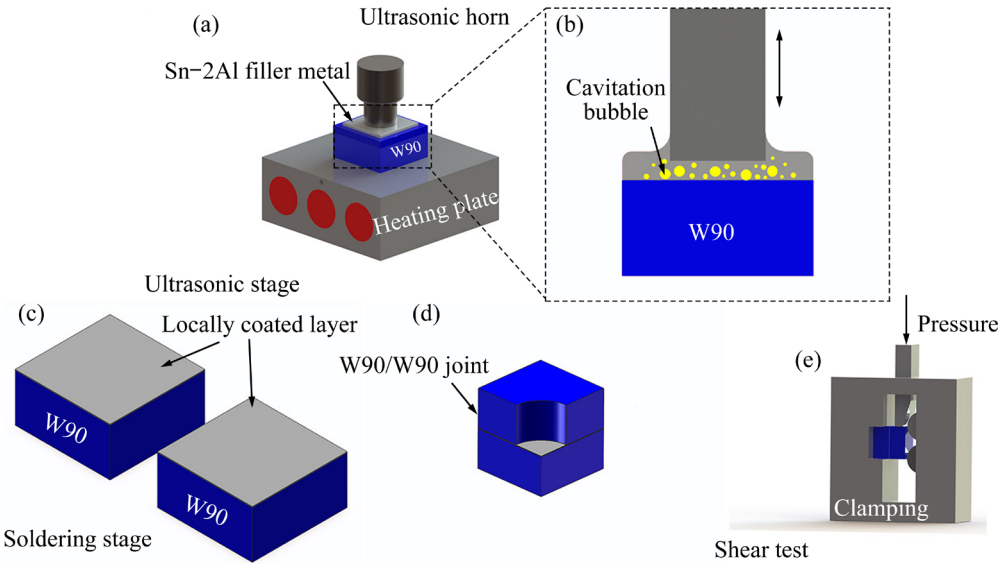

Fig. 1 Schematic diagrams for (a, b) ultrasonic-assisted coating process, (c, d) soldering process, and (e) shear test

ultrasonic head and Sn−2Al filler metal was 350 μm and the mass of Sn−2Al filler metal was approximately 200 mg. The ultrasonic power was 50, 100, 150 and 200 W. The ultrasonic time was set to be 6, 12, 18, 24 and 30 s, respectively. The locally coated W90 blocks of the same sizes (9 mm × 9 mm × 5 mm) were assembled face-to-face and soldered at 250 °C (Figs. 1(c, d)), followed by shear tests to determine the bonding strength.

2.2 Microstructure characterization and mechanical property analyses

The metallographic samples embedded in epoxy were sequentially ground with 400, 800, 1200 and 2000 grit silicon carbide paper, followed by polishing with 2.5 and 0.5 μm diamond paste in turn. The microstructures of the selected samples were analyzed by scanning electron microscopy (SEM, MERLIN Compact, ZEISS) equipped with energy disperse spectroscopy (EDS, OCTANE PLUS, EDAX). Shear tests were carried out by a universal testing machine (Instron 5967) at a constant crosshead speed of 0.5 mm/min (as shown in Fig. 1(e)). Five samples were selected for each group of process parameter and the average value was calculated. The fracture path and fracture surface were analyzed by SEM and X-ray diffraction (XRD, DX2700) with a step size of 0.02°.

3 Results

Figures 2(a−c) show the microstructures of Sn−2Al/W90 interface obtained at an ultrasonic power of 100 W and ultrasonic time of 6 s. The Sn−2Al filler metal on W90 surface appeared convex with a maximum thickness of approximately 500 μm after the ultrasonic treatment. This phenomenon was attributed to the adsorptive action between the ultrasonic head and the liquid filler metal during the lifting process of ultrasonic head. As shown in Fig. 2(a), the ultrasound promoted the wetting of Sn−2Al filler metal on W90 surface. The line scan results indicated that the Sn−2Al filler metal bonded well to W particles and (Ni,Fe) matrix (Figs. 2(d, e)). The Al_4W intermetallic compound (IMC) was formed at the Sn−2Al/W interface [19]. The Ni_3Sn_4 IMC was formed at the Sn−2Al/(Ni,Fe) matrix interface. In order to further observe the formation of Ni_3Sn_4 IMC, the temperature of ultrasonic-assisted coating process was increased to 450 °C and then the Sn−2Al filler metal was completely etched off. The result is shown in Fig. S1 in Supplementary Materials (SM) and the Ni_3Sn_4 IMC was found at the Sn−2Al/(Ni,Fe) matrix interface. Besides, the Sn−2Al filler metal was selectively melted onto W90 surface by controlling the migration of ultrasonic horn under the assistance of acoustic energy field, forming the geometry shown in Fig. 2(f).

To test the interfacial strength of Sn−2Al/W90 interface, the W90/Sn−2Al/W90 joint is prepared and Fig. 3 shows the microstructure and elemental distribution of W90/Sn−2Al/W90 joint treated with the ultrasonic power of 100 W and ultrasonic time of 6 s. Due to the gravity of W90, a lot of Sn−2Al filler metal was extruded from the seam and the

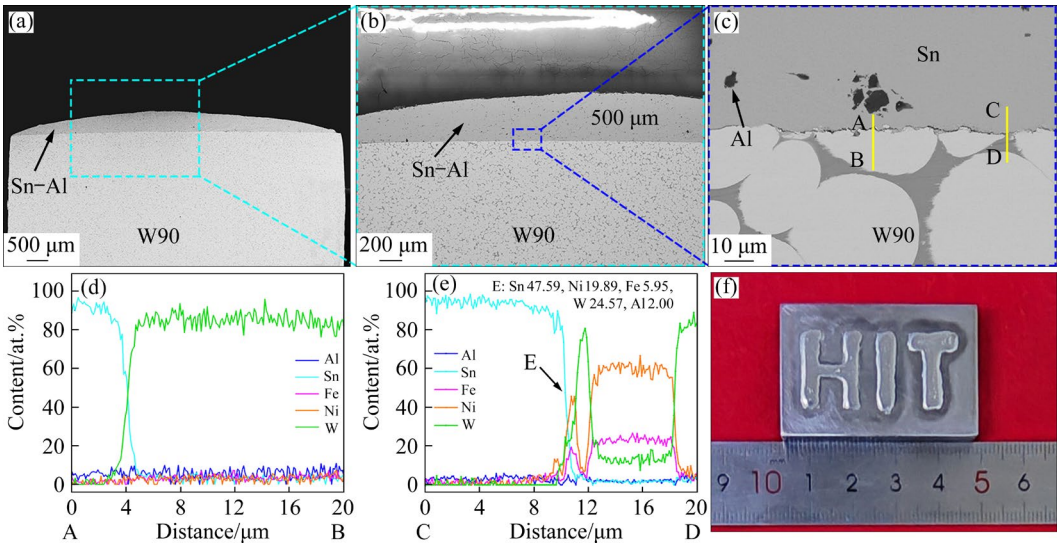

Fig. 2 Interfacial microstructures of Sn−2Al/W90 interface: (a−c) SEM images; (d, e) Line scan results of Lines AB and CD, respectively; (f) Pattern formed on W90 surface by selective ultrasonic-assisted coating process

width of seam was measured to be 40 μm. The formed seam was continuous with no cracks or cavities observed.

Figure 4 displays the effect of ultrasonic power and ultrasonic time on the microstructures of W90/Sn−2Al/W90 joints. It could be seen that the size of Al phase gradually decreased as the ultrasonic time increased from 6 to 30 s. Meanwhile, increasing ultrasonic power also shattered Al phases. It was worth noting that some broken regions were found at the Sn−2Al/W90 interface as the ultrasonic parameters were (150 W, 30 s), (200 W, 12 s), (200 W, 18 s), (200 W, 24 s) and (200 W, 30 s), as shown in the cyan circle.

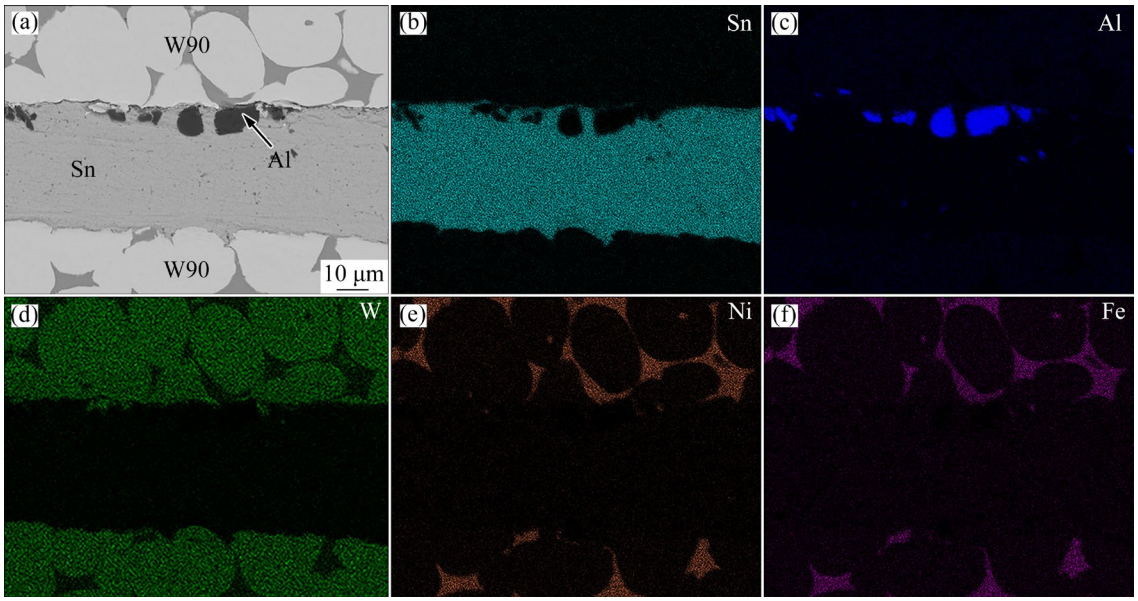

Fig. 3 Microstructure of W90/Sn−2Al/W90 joint treated with ultrasonic time of 6 s: (a) Interfacial microstructure; (b−f) EDS mapping scan results

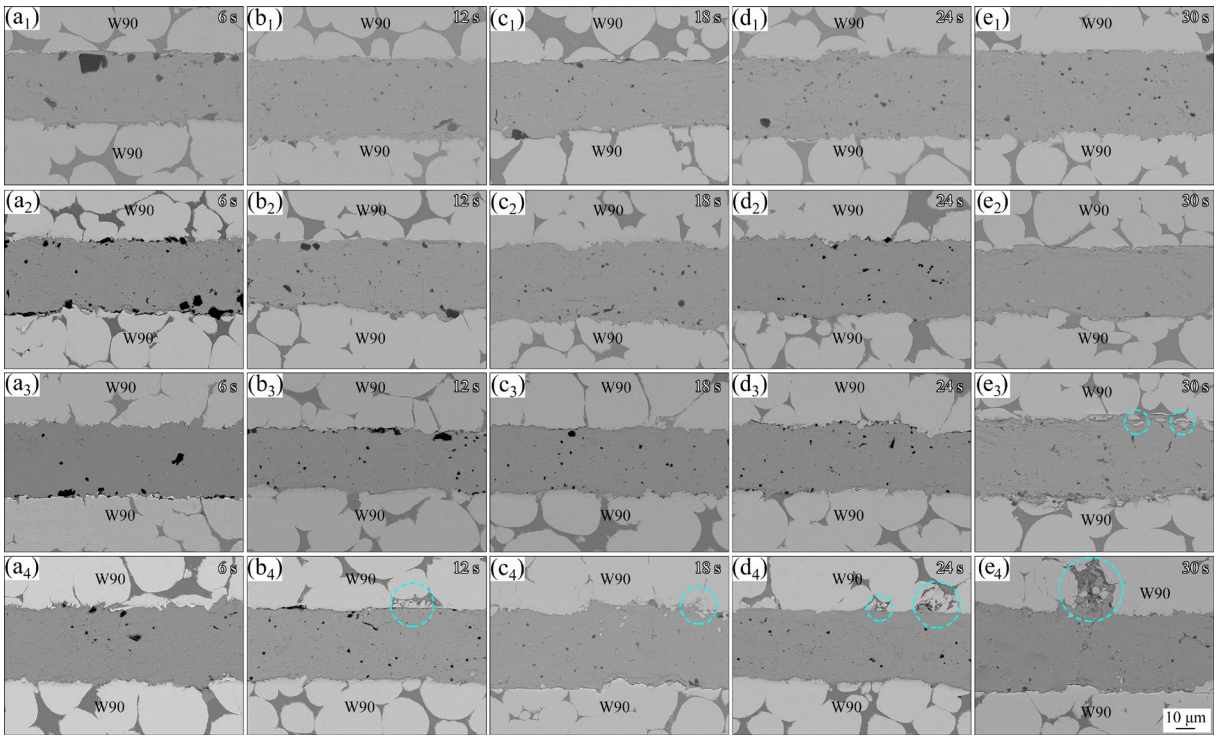

Fig. 4 Microstructures of W90/Sn−2Al/W90 joints treated with different ultrasonic power and ultrasonic time: (a_1−e_1) 50 W; (a_2−e_2) 100 W; (a_3−e_3) 150 W; (a_4−e_4) 200 W

Figure 5 shows the effects of the ultrasonic power and ultrasonic time on shear strength of W90/Sn−2Al/W90 joints. As the ultrasonic power increased from 50 to 200 W, the shear strength of joint gradually increased. The joint strength increased with the ultrasonic time increasing from 6 to 30 s as the ultrasonic powers were 50 and 100 W. As the ultrasonic powers were 150 and 200 W, the shear strength exhibited a trend of first increasing and then flattening, reaching a maximum value of 30.1 MPa.

In order to analyze the fracture positions of W90/Sn−2Al/W90 joints, the fracture surfaces of joints treated with the ultrasonic power of 100 W are shown in Fig. 6. As ultrasonic time increased from 6 to 30 s, the W90 area on the fracture surface deceased from 35.1% to 0% and the bonding area between Sn−2Al filler metal and W90 increased. As the ultrasonic time was 6 s, two areas were found on the fracture surface (Fig. 6(a)). The white area was the W90 area and the other area was the Sn−2Al filler metal area. With the ultrasonic time increasing to 24 s, the W90 area on the fracture surface decreased from 47.0% to 5.4%, indicating that more Al_4W phases at the Sn−2Al/W90 interface were formed and the interfacial bonding area increased. Only Sn−2Al filler metal was found on the fracture surface of joint treated with the ultrasonic time of 30 s (Fig. 6(e)). The joint fractured at the Sn−2Al filler metal (Fig. 6(f)). It was indicated that the Sn−2Al filler metal was fully bonded with W90 and the joint strength increased to 30.2 MPa. The XRD results of fracture surface also confirmed the phenomenon that the intensity of W peak gradually decreased and then disappeared as the ultrasonic time increased (Fig. 7). Besides, other fracture surfaces and XRD results of W90/Sn−2Al/W90 joints treated with 50, 150 and 200 W are shown in Supplementary Material (Figs. S2 and S3 in SM). It could be seen that increasing ultrasonic power decreased the W90 area on fracture surface and increased the bonding area of Sn−2Al/W90 interface, improving the interfacial strength. Therefore, the bonding area of Sn−2Al/W90 interface gradually increased as the ultrasonic power and ultrasonic time increased, resulting in the improvement of W90/Sn−2Al/W90 joint strength.

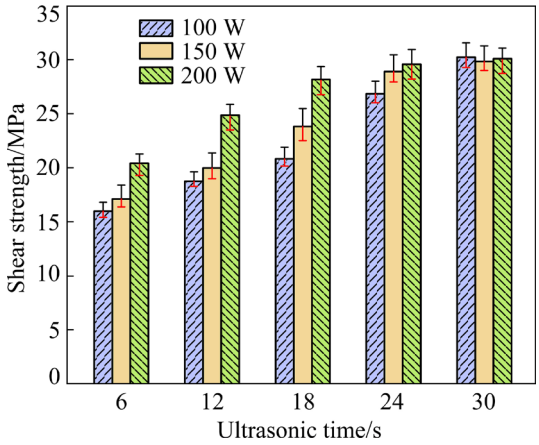

Fig. 5 Influence of ultrasonic power and ultrasonic time on shear strength of W90/Sn−2Al/W90 joint

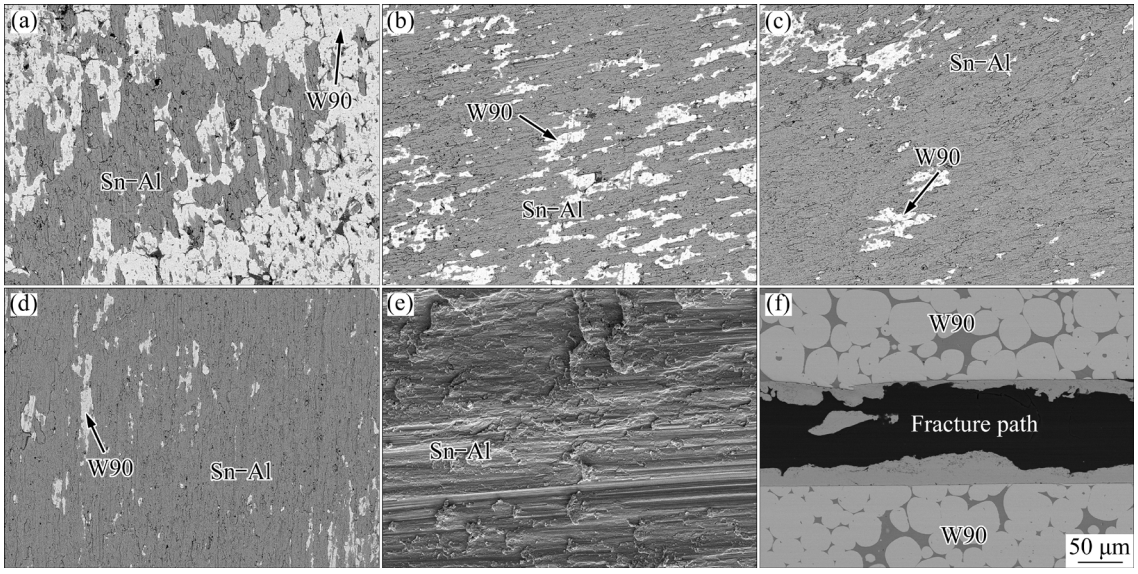

Fig. 6 Influence of ultrasonic time on fracture surface of W90/Sn−2Al/W90 joint treated with ultrasonic power of 100 W: (a) 6 s; (b) 12 s; (c) 18 s; (d) 24 s; (e, f) 30 s

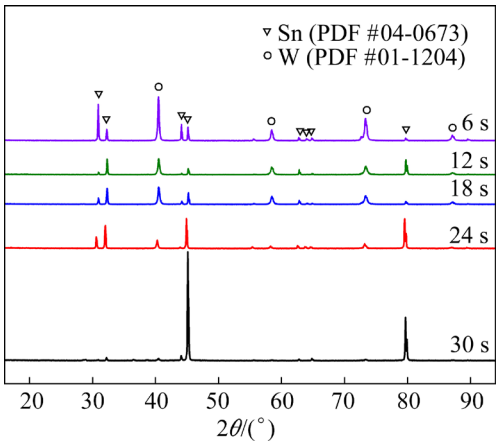

Fig. 7 XRD patterns of fracture surfaces of W90/Sn−2Al/W90 joints treated with 100 W at different ultrasonic time

4 Discussion

4.1 Acoustic pressure field inside Sn−2Al liquid metal

During ultrasonic-assisted coating process, the ultrasonic cavitation effect is crucial for the welding of dissimilar materials and the cavitation intensity is closely related to the acoustic pressure inside liquid metal [20,21]. The acoustic pressure inside Sn−2Al liquid metal was simulated by Comsol Multiphysics software. The solid mode had the same dimensions of 9 mm × 9 mm × 5 mm and the thickness of liquid mode was 350 μm as that in experiment, as shown in Fig. 8. The ultrasonic head was applied on the upper surface of Sn−2Al liquid metal. The diameter and frequency was the same as the experiment. The entire mode was meshed by 361996 units (Fig. 8(b)). The A point of (4.5, 4.5, 5) was selected to analyze the effect of ultrasonic power on the acoustic pressure inside Sn−2Al filler metal (Fig. 8(c)). The parameters used during calculation were as follows: the density of W90 was 17800 kg/m^3, the elasticity modulus of W90 was 3.6×10^{11} Pa, and the Poisson's ratio of W90 was 0.28; the sound velocity of Sn−2Al alloy was 2500 m/s, and the viscosity of Sn−2Al alloy was 0.0022 Pa·s.

In order to analyze the acoustic pressure variation of Sn−2Al/W90 interface during the ultrasonic-assisted coating process, the *XY* surface with *Z* value of 5 mm was extracted and the variation process of acoustic pressure field inside the liquid phase within the 9th period (400−450 μs) is shown in Fig. 9. The acoustic pressure inside the liquid phase was negative at the end of 8th period (400 μs). The acoustic pressure insider liquid phase evolved into positive values at 404 μs. The maximum positive pressure value of 0.61 MPa at the center of liquid phase and the pressure gradually decreased from the center position to the edge position (Fig. 9(b)). The acoustic pressure further increased and the maximum positive pressure value reached 19.8 MPa at 416 μs (Fig. 9(c)). The acoustic pressure began to decrease but remained positive at the end of positive half wave (425 μs) (Fig. 9(d)). As the sound wave entered into the negative half wave, the acoustic pressure changed into negative values at 430 μs (Fig. 9(e)). The acoustic pressure remained negative but had smaller values at the end of this acoustic period (450 μs) (Fig. 9(h)).

4.2 Effect of ultrasonic power on acoustic pressure and bubble dynamics

To study the effect of ultrasonic power on acoustic pressure inside liquid filler metal, Point A in Fig. 8(c) was chosen as the feature point and the acoustic pressure variation of Point A with the ultrasonic time increased, as shown in Fig. 10(a). The acoustic pressure curves showed sine-like

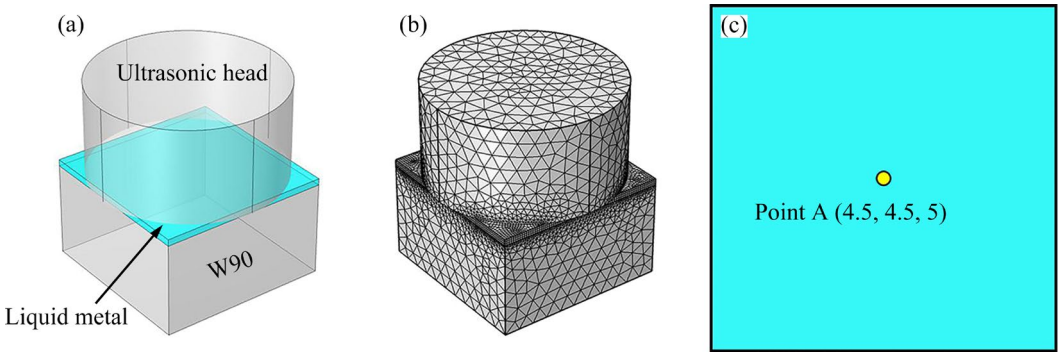

Fig. 8 (a, b) Acoustic pressure simulation mode and meshing; (c) Coordinate of feature point

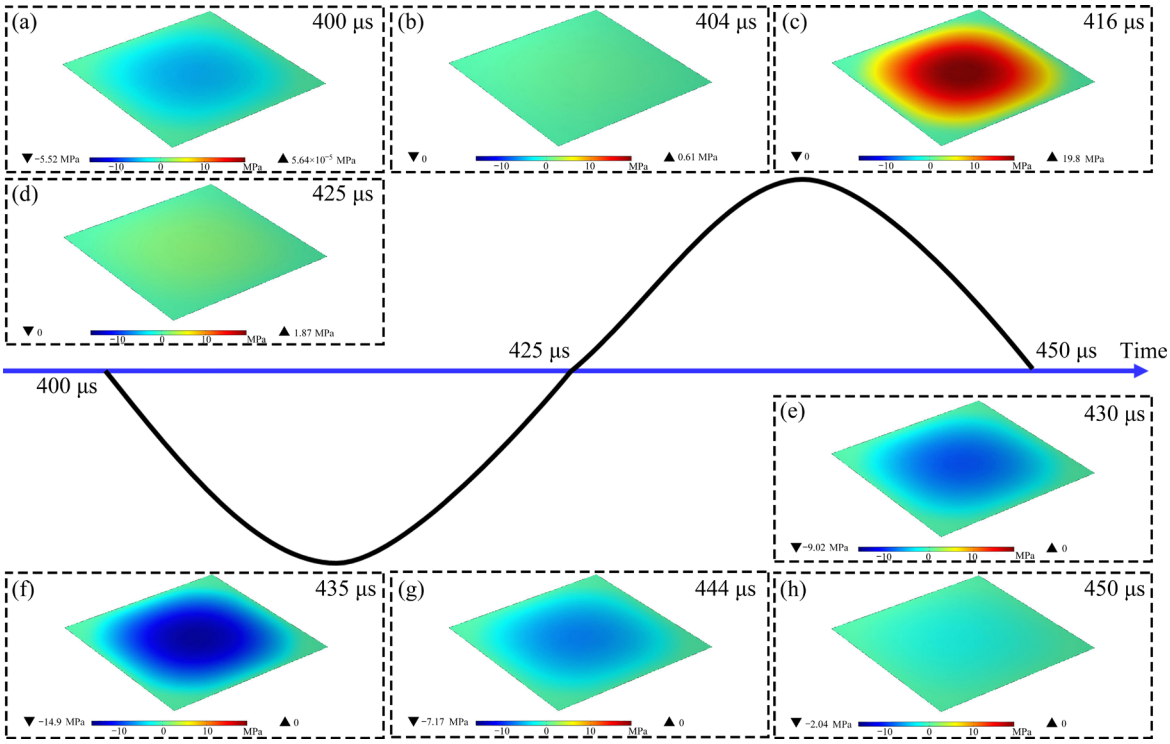

Fig. 9 Acoustic pressure field in liquid phase during ultrasonic-assisted coating process: (a) 400 μs; (b) 404 μs; (c) 416 μs; (d) 425 μs; (e) 430 μs; (f) 435 μs; (g) 444 μs; (h) 450 μs

morphologies and the maximum value of acoustic pressure gradually increased with the ultrasonic power increased from 50 to 200 W. In order to further analyze the action of improving ultrasonic power on acoustic pressure, the data of the 4th period were extracted and the extracted acoustic pressure was fitted by Origin software.

The fitted acoustic pressure equations were listed in Eqs. (1), (2), (3) and (4), respectively corresponding to the ultrasonic power of 50, 100, 150 and 200 W:

$$P_1=0.12+8.22\sin\left[2\pi\times20000\times\left(t-4.00\times10^{-6}\right)\right] \quad (1)$$

$$P_2=0.24+16.44\sin\left[2\pi\times20000\times\left(t-4.00\times10^{-6}\right)\right] \quad (2)$$

$$P_3=0.36+24.66\sin\left[2\pi\times20000\times\left(t-4.00\times10^{-6}\right)\right] \quad (3)$$

$$P_4=0.48+32.88\sin\left[2\pi\times20000\times\left(t-4.00\times10^{-6}\right)\right] \quad (4)$$

which follow the format:

$$P=P_0+P_A\sin\left[2\pi f\left(t-t_0\right)\right] \quad (5)$$

where P is the transient acoustic pressure, P_A is the amplitude of acoustic pressure, P_0 is the offset of sinusoidal curve, f is the frequency and t_0 is the initial time. It could be seen that the variation frequency of acoustic pressure inside the Sn−2Al liquid filler metal was consistent with that of ultrasonic wave and the sinusoidal acoustic pressure curve was negatively offset. The maximum value of acoustic pressure was 8.34, 16.68, 25.02 and 33.36 MPa, respectively, corresponding to 50, 100, 150 and 200 W. Therefore, we can infer that the ultrasonic-assisted coating technology does not alter the frequency of acoustic pressure inside the liquid phase and improving the ultrasonic power can increase the maximum value of acoustic pressure.

The ultrasonic cavitation effect is actually the emerge−growth−shrink−collapse process of cavitation bubble, in which the high temperature, high pressure and micro-jets are generated. To further investigate the mechanism of ultrasonic cavitation effect on the formation of W90/Sn−2Al/W90 joint, we used the Keller−Miksis (K−M) equation to study the bubble dynamics:

$$\left(1-\frac{\mathrm{d}R}{\mathrm{d}t}\frac{1}{c}\frac{\mathrm{d}R/\mathrm{d}t}{c}\right)R\frac{\mathrm{d}^2R}{\mathrm{d}t^2}+\frac{3}{2}\left(\frac{\mathrm{d}R}{\mathrm{d}t}\right)^2\left(1-\frac{\mathrm{d}R}{\mathrm{d}t}\frac{1}{3c}\right)=\frac{1}{\rho}\left[\left(1+\frac{\mathrm{d}R}{\mathrm{d}t}\frac{1}{c}\right)P_1+\frac{R}{c}\frac{\mathrm{d}P_1}{\mathrm{d}t}\right] \quad (6)$$

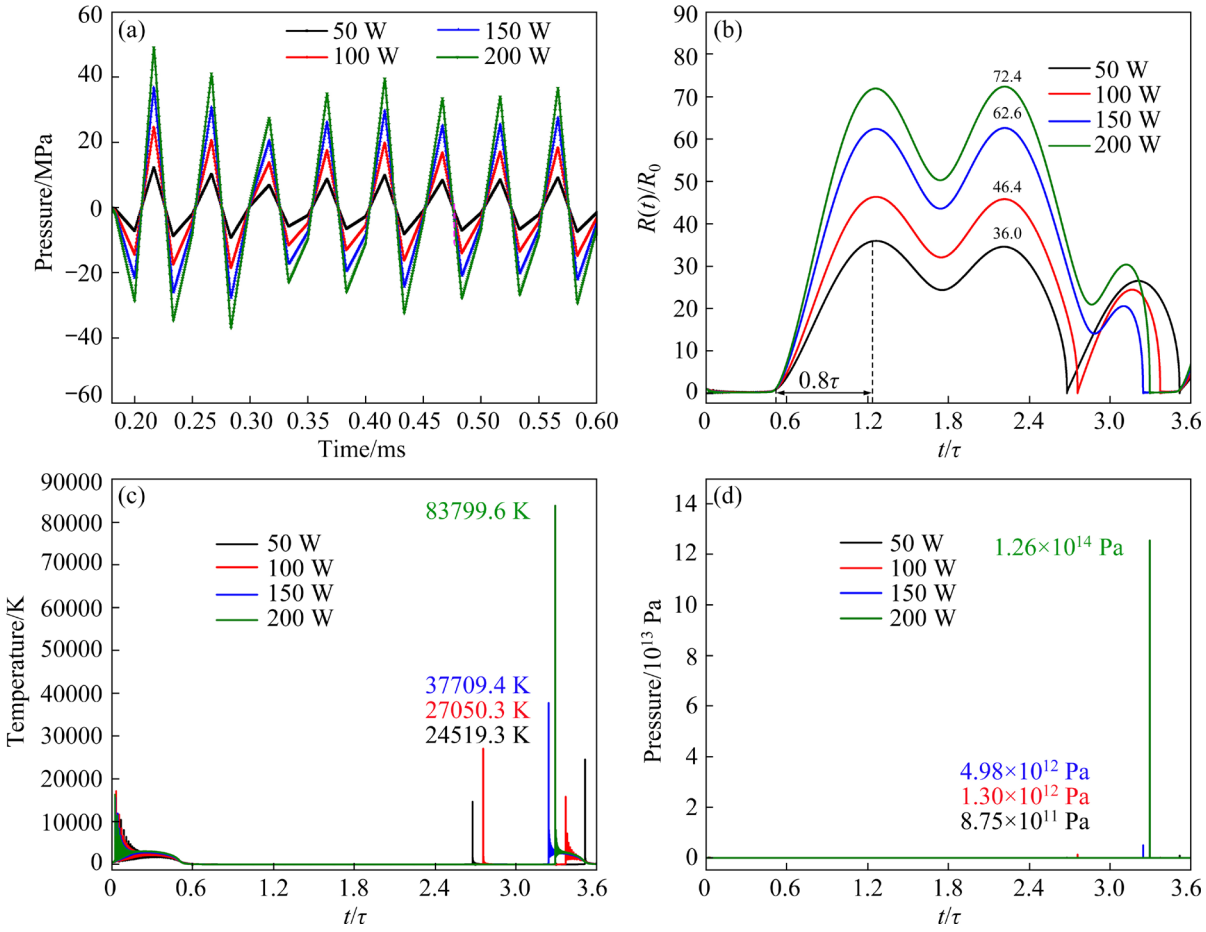

Fig. 10 (a) Effect of ultrasonic power on pressure of Point A; (b) Solution $R(t)/R_0$ within two acoustic periods, (c) temperature and (d) pressure of bubble collapse

$$P_1=\left(P_0+\frac{2\sigma}{R_0}-P_v\right)\left(\frac{R_0}{R}\right)^{3k}+P_v-P_0-\frac{4\mu}{R}\frac{\mathrm{d}R}{\mathrm{d}t}-\frac{2\sigma}{R}-P_A\sin(2\pi ft) \quad (7)$$

where c is the sound velocity in liquid filler metal; ρ is the density of liquid filler metal; σ is the surface tension of liquid filler metal; R_0 is the initial diameter of cavitation bubble; R is the instantaneous radius of cavitation bubble; P_v is the vapor pressure of liquid filler metal; μ is the viscosity coefficient of liquid filler metal; k is the exponent reflecting the thermodynamic state of cavitation bubble. Suppose that the gas inside the cavitation bubble was air and k=1.33. Given that Eq. (6) was a second-order ordinary differential equation, obtaining an analytical solution was difficult. Therefore, we used the fourth Runge−Kutta method to obtain a numerical solution.

In this work, Sn−2Al filler metal was used to bond W90 and the matrix of Sn−2Al metal was β-Sn. We ignored the effect of Al phase on the growth and collapse of cavitation bubble during the bubble dynamics calculation. The nucleation diameter of cavitation bubble was assumed to be 20 μm [22,23]. Figure 10(b) shows the bubble dynamics within two acoustic periods at different ultrasonic powers. The abscissa represents the ratio of ultrasonic time (t) to period (τ). The ordinate represents the ratio of bubble diameter ($R(t)$) to initial diameter (R_0). It could be found that all cavitation bubbles grew rapidly after approximately 0.5τ. As the ultrasonic power was 50 W, the bubble grew to 36.0 times of its initial size within 0.8τ. The cavitation bubble lives, from the bubble nucleation to collapse, were approximately from the bubble nucleation to collapse, only 2.2τ. In particular, $R(t)/R_0$ increased to 46.4, 62.6 and 72.4 as the ultrasonic power was 100, 150 and 200 W, respectively. The cavitation bubble lives gradually decreased as the ultrasonic power increased. Figure S5 in SM shows the velocities of bubble wall when bubble collapsed. The bubble had a

collapse wall velocity of 8216.8 m/s as the ultrasonic power was 50 W. The collapse velocity of bubble formed under the ultrasonic power of 100, 150 and 200 W was approximately 8499.2, 46353.2 and 6599.8 m/s, respectively. Such large velocities of bubble wall could lead to shock wave with large energy and pressure [24], which could break the oxide layer directly and etch the surface of materials.

The collapse of bubble creates an extremely non-equilibrium physicochemical environment and holds great potential for high-temperature and high-pressure chemical reaction [15]. In order to know the high temperature and high pressure generated by bubble collapse, the high-temperature value (T) and high-pressure value (P) by Eqs. (8) and (9), respectively:

$$T = T_0\left(\frac{R_0}{R}\right)^{3(k-1)} \tag{8}$$

$$P = (P_0 + \frac{2\sigma}{R_0} - P_v)\left(\frac{R_0}{R}\right)^{3k} \tag{9}$$

where T_0 is the initial temperature of liquid filler metal. Figure 10(c) shows the temperature generated by the collapse of cavitation bubble. As the ultrasonic power was 50 W, the collapse of cavitation bubble produced a high temperature of 24519.3 K. The collapse temperature increased to 27050.3, 37709.4 and 83799.6 K when the ultrasonic power increased to 100, 150 and 200 W, respectively. Such high temperature was obviously higher than the melting temperature of W90 (3673 K), but the generation of high temperature was instantaneous and the transfer of heat was extremely fast, which was difficult to melt W90. The melting phenomenon on the W90 surface was not found (Fig. 4). Another particular phenomenon caused by bubble collapse was high pressure and the results of calculated pressure is shown in Fig. 10(d). The cavitation bubble formed in the ultrasonic power of 50 W resulted into the high pressure of 8.75×10^{11} Pa. The pressure further increased to 1.30×10^{12}, 4.98×10^{12} and 1.26×10^{14} Pa when the ultrasonic power increased to 100, 150 and 200 W, respectively. The high pressure could directly break the oxide layer and the surface of W90 during the ultrasonic-assisted coating process.

During a cycle of sound wave, the cavitation bubbles in liquid phase nucleated and grew at the negative pressure period and contracted or collapsed at the positive period. As the acoustic pressure evolved into the next cycle, a new bubble emerge−growth−shrink−collapse process might continue to occur [25]. Therefore, extending the ultrasonic time can improve the probability of cavitation effect at the Sn−2Al/W90 interface and increasing the ultrasonic power can improve the intensity of cavitation effect.

The breakage of W90 demonstrated the generation of shock wave and micro-jet by the collapse of cavitation bubble (Fig. 4). The generated high temperature and high pressure promoted the formation of Al_4W IMC at the Sn−2Al/W90 interface [19]. In order to observe the cavitation effect of different parameters, the Sn−2Al filler metal on W90 after ultrasonic-assisted coating process was etched off by the 10% HNO_3 solution. The corresponding results at different ultrasonic time and ultrasonic power are shown in Fig. 11 and Fig. 12, respectively. The degree of breakage of W90 surface represented the intensity of cavitation effect. Figure 11 shows the effect of ultrasonic time on the surface morphology of W90 and the ultrasonic power is 100 W. According to the EDS results (Table 1), it could be observed that the surface of W particle was not damaged and some cracks were found in the (Ni,Fe) matrix. This was attributed to the higher hardness of W particle. Some corrosive liquid residues were seen on the surface of W particle. As the ultrasonic time increased from 6 to 30 s, the number of cracks in the (Ni,Fe) matrix increased and the (Ni,Fe) matrix was removed from the W90, exposing the next layer of W particles. It was indicated that more cavitation effect occurred at the Sn−2Al/W90 interface with the increase of ultrasonic time. It was worth noting that a pit was observed at the W90 surface as the ultrasonic time was 24 s. The size of pit was about 10 μm. The effect of ultrasonic power on the surface morphology of W90 is shown in Fig. 12. As the ultrasonic power increased from 50 to 200 W, the breakage of (Ni,Fe) matrix was aggravated. As the ultrasonic power was 150 W, partial (Ni,Fe) matrix was detached from the W90 and some fatigue striations were found at the bottom of (Ni,Fe) matrix (Fig. 12(b_1)). The fatigue striation was the characteristic of cavitation erosion [26]. The cavitation intensity was proportion to the ultrasonic power, which was consistent with the calculated results.

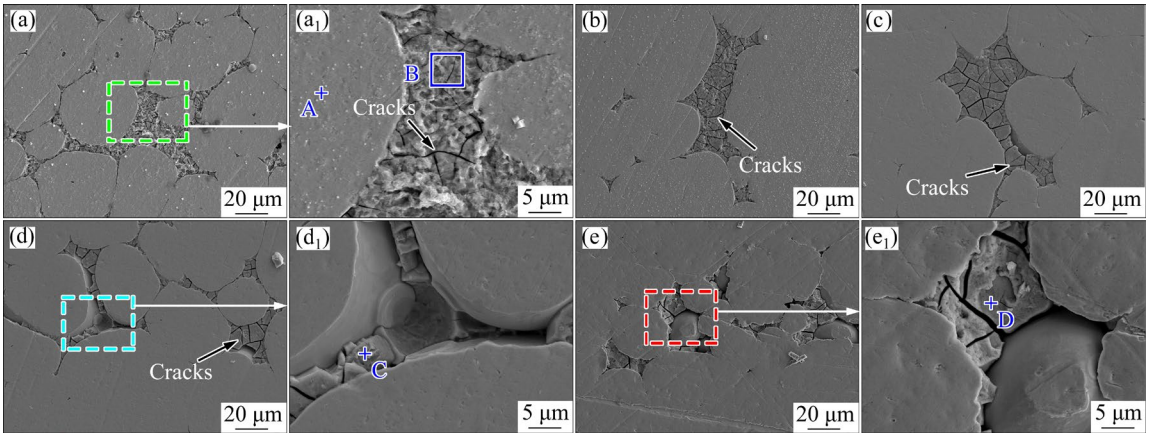

Fig. 11 Effect of ultrasonic time on surface morphology of W90 with ultrasonic power of 100 W: (a, a_1) 6 s; (b) 12 s; (c) 18 s; (d, d_1) 24 s; (e, e_1) 30 s

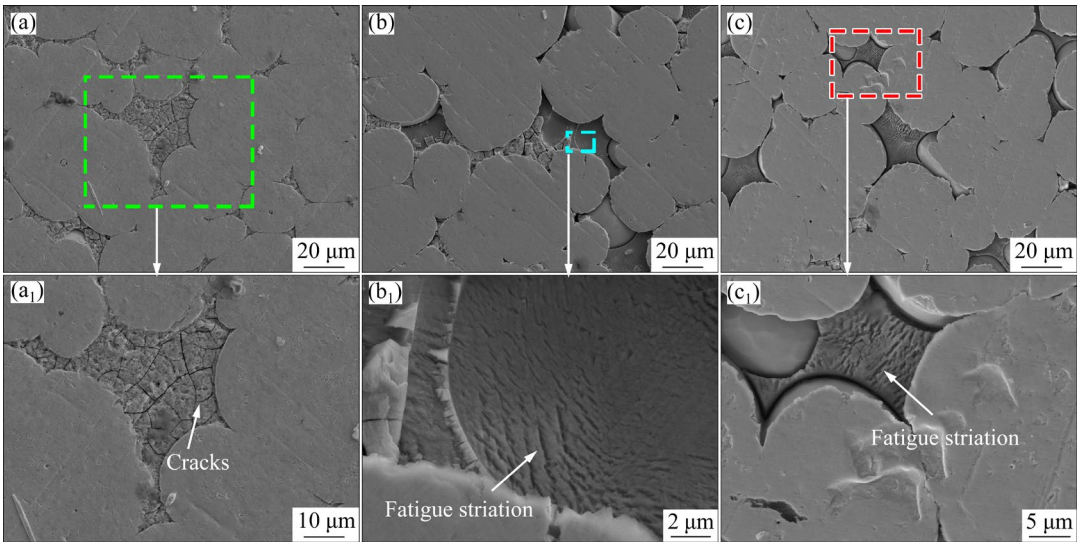

Fig. 12 Effect of ultrasonic power on surface morphology of W90 with ultrasonic time of 18 s: (a, a_1) 50 W; (b, b_1) 150 W; (c, c_1) 200 W

Table 1 Elemental compositions of different phases in Fig. 11 (at.%)

Position	W	Ni	Fe	Sn	Al	Possible phase
A	99.74	0.07	0.06	0.12	0.01	W
B	30.85	34.75	34.35	0.03	0.02	(Ni,Fe) matrix
C	58.50	16.78	20.27	4.43	0.02	W
D	85.19	5.74	8.96	0.09	0.02	W

Figures 11 and 12 confirm that the collapse of cavitation bubble can generate an extreme conditions, such as high temperature, high pressure and shock wave. The extreme conditions provide an environment for the formation of Al_4W during ultrasonic-assisted coating process. However, higher ultrasonic power causes the higher intensity of cavitation effect, which easily breaks the W90 base metal.

4.3 Formation mechanism of W90/Sn−2Al/Mg joint

From the above discussion, the formation mechanism of Sn−2Al coating on W90 surface is summarized in Fig. 13. When the temperature rose to 250 °C, the Sn−2Al filler metal melted but was

not wet on the surface of W90 (Fig. S4 in SM and Fig. 13(a)). Then, the ultrasound was applied on the surface of molten Sn−2Al filler metal and the wetting and spreading of Sn−2Al filler metal on W90 surface occurred. Meanwhile, the ultrasonic vibration appeared inside the Sn−2Al liquid metal and acoustic pressure gradually varied at different positions, resulting into the growth and contraction of cavitation bubble in a cycle (Fig. 13(b)). As the acoustic pressure value exceeded the cavitation threshold (1.26 MPa) [23], the cavitation bubble collapsed at the positive period and the cavitation effect occurred at the Sn−2Al liquid metal. The cavitation effect occurred at the liquid/solid interface, creating an extremely non-equilibrium physicochemical environment along with micro-jet, high temperature, high pressure and shock wave. The generated micro-jet and shock wave near the Al phases broke them to pieces and the size of Al phase decreased. The cavitation effect at the Sn−2Al/W90 interface provided an extreme environment for the chemical reaction between Al and W atoms and generated the micro-jet and shock wave to etch the W90 surface. Some etched pits existed on the W90 surface (Fig. 13(c)). Under the action of cavitation effect, the Al_4W IMC was formed at the Sn−2Al/W90 interface and Ni_3Sn_4 IMC was formed at the Sn−2Al/(Ni,Fe) matrix phase interface. Finally, the heating plat and the ultrasonic vibration were turned off. Due to the adsorptive action between ultrasonic head and liquid metal, the surface Sn−2Al liquid metal became convex during the lifting process of ultrasonic head (Fig. 13(d)).

The intensity of ultrasonic cavitation effect is closely related with the acoustic pressure inside liquid metal [21]. The acoustic pressure value inside Sn−2Al liquid metal was proportional to the ultrasonic power, as shown in Fig. 10(a). As the ultrasonic power was 50 W, the acoustic pressure value inside Sn−2Al liquid metal was lower, resulting into weaker cavitation effect at the liquid/solid interface. The size of Al phase was obviously larger and the size of etched pits became small (Fig. 13(e)). Some unbonded area existed at the Sn−2Al/W90 interface, decreasing the interfacial strength (Fig. 5). As the ultrasonic power increased to 150 and 200 W, stronger cavitation effect occurred at the liquid/solid interface and the size of Al phase was smaller. The size of etched pits increased. Besides, the acoustic pressure inside Sn−2Al liquid metal was variable in one period and

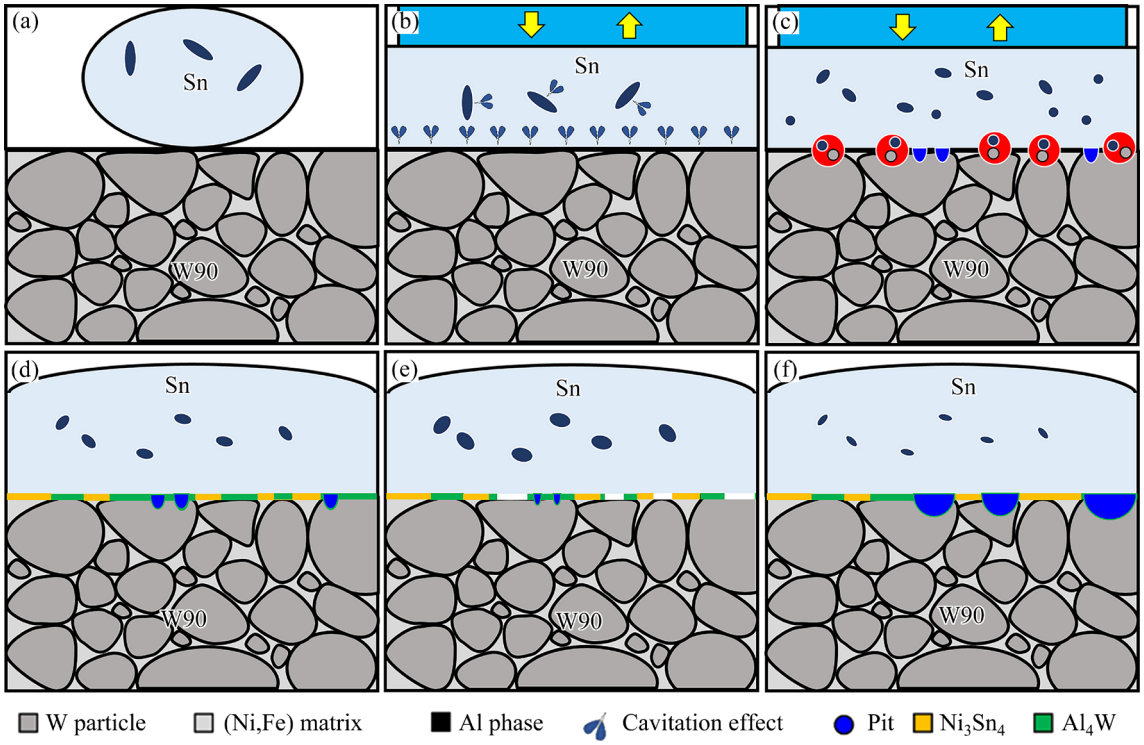

Fig. 13 Schematic diagram of formation mechanism of Sn−2Al coating on W90 via ultrasonic cavitation effect: (a) Before applying ultrasound; (b, c) Ultrasonic stage; (d) Cooling stage; (e) Weak cavitation effect; (f) Strong cavitation effect

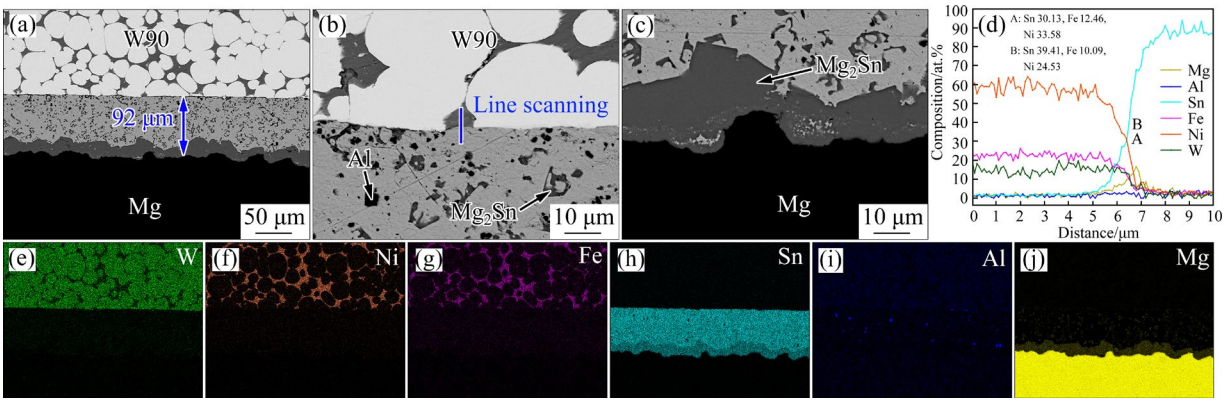

Fig. 14 (a−c) Interfacial microstructure of W90/Sn−2Al/Mg joint treated with ultrasonic time of 6 s and ultrasonic power of 100 W; (d) Line scan result of blue line in (b); (e−j) EDS mapping scan results in (a)

increasing the ultrasonic time was conducive to the occurrence of cavitation effect at the Sn−2Al/W90 interface, which promoted the interfacial bonding and improved the interfacial strength (Fig. 5).

4.4 Comparison of ultrasonic-assisted soldering and ultrasonic-assisted coating technologies

As previously mentioned, an important advantage of ultrasonic-assisted coating technology is the prevention of excessive growth of IMC. In previous work, W90 tungsten heavy alloy and AZ31B Mg alloy were successfully bonded by ultrasonic-assisted soldering using Sn−Al filler metal [19,27]. As the ultrasonic time was 6 s, the joint strength reached the maximum value of 24.6 MPa. The joint fractured at two positions: W90/Sn−Al interface and filler metal. But it was difficult to further improve the joint strength by increasing ultrasonic power. The ultrasound could promote the Mg atom diffusion [28] and the improvement of ultrasonic power increased the thickness of Mg_2Sn layer, decreasing the joint strength. Therefore, the ultrasonic-assisted coating technology was proposed to further improve the W90/Sn−Al/Mg joint strength.

The parameters for ultrasonic-assisted coating process of W90 were selected as follows: ultrasonic power of 100 W, ultrasonic time of 30 s and heating temperature of 250 °C. Figure 14 shows interfacial microstructure of W90/Sn−2Al/Mg joint. The soldering temperature, ultrasonic power and ultrasonic power were 250 °C, 100 W and 6 s, respectively. The joint width was measured to be 92 μm. On the Mg side, a wavy interface was found and a Mg_2Sn layer was formed, indicating the removal of oxide film on the surface of Mg alloy. The microstructure of W90/Sn−2Al/Mg joint was composed of W90/Sn+Mg_2Sn/Mg_2Sn layer/Mg. The shear strength of joint was 33.9 MPa, which was obviously higher than that bonded by ultrasonic-assisted soldering technology [19]. The results confirm the effectiveness of ultrasonic-assisted coating technology, highlighting its potential for improving the joint strength in low-temperature bonding tungsten heavy alloy and other metals.

5 Conclusions

(1) The Sn−2Al coating was successfully achieved on W90 substrate assisted with ultrasound in atmospheric environment at 250 °C. As the ultrasonic power increased from 50 to 200 W and ultrasonic time increased from 6 to 30 s, the size of Al phase decreased and the bonding area of Sn−2Al/W90 increased. After Sn−2Al filler metal was etched off, the number and size of pits on the W90 surface increased.

(2) Acoustic pressure presented alternating negative and positive characteristics in one period. As the ultrasonic power increased, the maximum value of acoustic pressure increased from 8.34 to 33.36 MPa, the high temperature generated by the collapse of cavitation bubble increased from 24519.3 to 83799.6 K and the high pressure increased from 8.75×10^{11} to 1.26×10^{14} Pa.

(3) As the ultrasonic power and ultrasonic time increased, the W90 area on fracture surface decreased and the bonding area between Sn−2Al filler metal and W90 increased, resulting into the

increase of interfacial strength. The maximum value of Sn−2Al/W90 interfacial strength reached 30.1 MPa.

(4) Compared with the ultrasonic-assisted soldering technology, the ultrasonic-assisted coating technology has the obvious advantages in the bonding of W90 and Mg alloy. The shear strength of W90/Sn−2Al/Mg joint by ultrasonic-assisted coating technology reached 33.9 MPa, which was obviously higher than that bonded by ultrasonic-assisted soldering technology.

CRediT authorship contribution statement

Xiao-guo SONG: Conceptualization, Supervision, Methodology; **Xu-dong ZHANG:** Data curation, Investigation, Writing − Original draft; **Wei FU:** Writing − Review & editing, Supervision, Funding acquisition; **Xiao-yu TIAN:** Supervision, Funding acquisition, Resources; **Guang-dong WU:** Resources, Supervision; **Sheng-peng HU:** Conceptualization, Methodology, Validation.

Declaration of competing interest

The authors declare that they have no known competing financial interests or personal relationships that could have appeared to influence the work reported in this paper.

Acknowledgments

This work was supported by the National Natural Science Foundation of China (Nos. 52105330, 52175307), and the Natural Science Foundation of Shandong Province, China (No. ZR2023JQ021).

Supplementary Materials

Supplementary Materials in this paper can be found at: https://tnmsc.csu.edu.cn/download/17-p0259-2024-0582-Supplementary_Materials.pdf.

References

[1] WU Yuan-bing, ZHAO Jian-hua, PENG Wei-li, GU Cheng, CHENG Jin, WANG Ya-jun. Optimization of additive manufactured Ti-based pyramidal lattice structure applied to interface strengthening of Mg/Ti bimetal composites [J]. Transactions of Nonferrous Metals Society of China, 2024, 34(3): 846−860.

[2] LI Jie, SHI Lei, LI Yi-nan, ZHOU Tao-shuai, YU Zi-jing, ZHANG Hong-chang, PENG Zi-long, MIAO Shu-wen, GAO Jian-guo, SU Zhao-fang. Reinforcement effect of Mg−Al−Zn ternary IMC on MB8/2024 joints with Al/Zn/Cu/Zn multi-interlayer via ultrasonic-assisted brazing [J]. Transactions of Nonferrous Metals Society of China, 2023, 33(4): 1015−1028.

[3] WANG Guang-hong, QU Sheng-guan, HE Rui-liang, HU Ke, LI Xiao-qiang. Effect of carburization on microstructure and rolling contact fatigue property of 95W−3.4Ni−1.6Fe heavy alloy [J]. Transactions of Nonferrous Metals Society of China, 2016, 26(12): 3161−3169.

[4] LI Xiao-qiang, XIN Hong-wei, HU Ke, LI Yuan-yuan. Microstructure and properties of ultra-fine tungsten heavy alloys prepared by mechanical alloying and electric current activated sintering [J]. Transactions of Nonferrous Metals Society of China, 2010, 20(3): 443−449.

[5] LU Da-shi, YOU Guo-qiang, PENG Li-zhen, YAO Fan-jin, ZHOU Kai-xuan. Microstructures and properties of a multilayered Al/W composite fabricated for γ-ray-shielding applications [J]. Radiation Physics and Chemistry, 2022, 198: 110209.

[6] SHANG Jian-li, YAN Jia-zhen, LI Ning. Brazing W and Fe−Ni−Co alloy using Ag−28Cu and Ag−27Cu−3.5Ti fillers [J]. Journal of Alloys and Compounds, 2014, 611: 91−95.

[7] XIA Chun-zhi, SUN Wei-wei, ZHOU Yi, ZHAO Meng. Effect of Ni−Ti filler on brazed W−Cu/18-8 joints [J]. Journal of Materials Processing Technology, 2018, 259: 15−22.

[8] DONG Hong-jie, LI Zhuo-lin, SONG Xiao-guo, FENG Ji-cai, WEI Shou-jing, FU Jun-hong, SHI Yue. Ultrasonic-based surface patterning and interfacial reaction of ZrO_2 ceramics [J]. Journal of Materials Science & Technology, 2023, 155: 202−210.

[9] GUO Wei-bing, LUAN Tian-min, LENG Xue-song, HE Jing-shan, YAN Jiu-chun. Interfacial microstructure evolution and mechanical properties of Al/Sn joints by ultrasonic-assisted soldering [J]. Transactions of Nonferrous Metals Society of China, 2017, 27(4): 962−970.

[10] DONG Fang, LI Xiao-qian, ZHANG Li-hua, MA Li-yong, LI Rui-qing. Cavitation erosion mechanism of titanium alloy radiation rods in aluminum melt [J]. Ultrasonics Sonochemistry, 2016, 31: 150−156.

[11] DAI Xiang, SHI Lei, TIAN Chun-yan, WU Chuan-song, GAO Song. Effect of ultrasonic vibration on microstructures and mechanical properties of friction stir welded 2195 Al−Li alloy [J]. Transactions of Nonferrous Metals Society of China, 2024, 34(1): 80−93.

[12] BRUJAN E A. Shock wave emission and cavitation bubble dynamics by femtosecond optical breakdown in polymer solutions [J]. Ultrasonics Sonochemistry, 2019, 58: 104694.

[13] MA Xiao-jian, HUANG Biao, ZHAO Xin, WANG Yue, CHANG Qing, QIU Si-cong, FU Xiao-ying, WANG Guo-yu. Comparisons of spark-charge bubble dynamics near the elastic and rigid boundaries [J]. Ultrasonics Sonochemistry, 2018, 43: 80−90.

[14] GAO Xiao-lei, CHEN Chao. High-strength joining of silica glass and 2024 aluminum alloy by ultrasonic-assisted soldering with Sn−Bi low temperature solder [J]. Journal of Manufacturing Processes, 2023, 101: 1482−1496.

[15] PRIYADARSHI A, KHAVARI M, SUBROTO T, CONTE M, PRENTICE P, PERICLEOUS K, ESKIN D,

DURODOLA J, TZANAKIS I. On the governing fragmentation mechanism of primary intermetallics by induced cavitation [J]. Ultrasonics Sonochemistry, 2021, 70: 105260.

[16] DONG Hong-jie, LI Zhuo-lin, SONG Xiao-guo, GUO Xia-jun, LUO Yan-xu, BAI Tian-sheng, WEI Shou-jing, ZHAO Hong-yun, YAN Jiu-chun, FENG Ji-cai. Low-temperature ultrasound-activated joining of ZrO_2 ceramics using Sn−Al−Cu solder [J]. Journal of American Ceramic Society, 2019, 102(5): 2272−2277.

[17] DONG Hong-jie, WEI Shou-jing, LI Zhuo-lin, SONG Xiao-guo, HE Wen-xiong, FENG Ji-cai. In-situ formation of amorphous Al_2O_3 interphase during ultrasonic-assisted soldering process of ZrO_2 ceramic and 1060Al using Sn filler at low temperature [J]. Surfaces and Interfaces Journal, 2023, 36: 102491.

[18] XU Yan, MA Xin-ran, TANG Hao-yang, YAN Jiu-chun. Mechanism of the interfacial reaction between sapphire and Sn−3.5Ag−4Ti solder at a low temperature in air by ultrasound [J]. Ceramics International, 2020, 46(4): 4435−4443.

[19] ZHANG Xu-dong, FU Wei, SONG Xiao-guo, CHEN Liang-bo, LI Zhuo-lin, HU Sheng-peng, BIAN Hong. Ultrasonic-assisted soldering W90 Tungsten heavy alloy to AZ31B Mg alloy using Sn−*x*Al alloy [J]. Journal of Materials Science & Technology, 2024, 175: 132−140.

[20] RIEDEL E, MARTIN L, SCHARF S. Simulation of ultrasonic induced cavitation and acoustic streaming in liquid and solidifying aluminum [J]. Metals, 2020, 10: 476.

[21] LI Zhen-wei, XU Zhi-wu, MA Lin, WANG Sheng, LIU Xue-song, YAN Jiu-chun. Cavitation at filler metal/substrate interface during ultrasonic-assisted soldering. Part I: Cavitation characteristics [J]. Ultrasonics Sonochemistry, 2018, 49: 249−259.

[22] LI Guo-kui, ZHAO Yu, LI Jia-qi, XIAO Yong. Evolution behavior of cavitation bubble in pure Sn liquid medium with narrow gap under low-amplitude ultrasound [J]. Ultrasonics Sonochemistry, 2023, 99: 106567.

[23] LI Zheng-wei, XU Zhi-wu, HE Peng, MA Zhong-wei, CHEN Shu, YAN Jiu-chun. Dependence of wetting on cavitation during the spreading of a filler droplet on the ultrasonically agitated Al substrate [J]. Ultrasonics Sonochemistry, 2022, 82: 105893.

[24] BRUJAN E A, IKEDA T, MATSUMOTO Y. On the pressure of cavitation bubbles [J]. Experimental Thermal and Fluid Science, 2008, 32(5): 1188−1191.

[25] LI Zheng-wei, XU Zhi-wu, ZHAO De-gang, CHEN Shu, YAN Jiu-chun. Ultrasonic cavitation at liquid/solid interface in a thin Ga−In liquid layer with free surface [J]. Ultrasonics Sonochemistry, 2021, 71: 105356.

[26] DU Jian-hua, CHEN Feng-jun. Cavitation dynamics and flow aggressiveness in ultrasonic cavitation erosion [J]. International Journal of Mechanical Sciences, 2021, 204: 106545.

[27] ZHANG Xu-dong, FU Wei, SONG Xiao-guo, LI Zhuo-lin, LONG Wei-min, LIN Dan-yang, SONG Yan-yu, ZHONG Su-juan. Ultrasonic-induced metallurgical bonding between W90 tungsten heavy alloy and AZ31B Mg alloy using Sn [J]. Materials Letters, 2023, 352: 135175.

[28] ZHANG Xu-dong, FU Wei, ZHANG Jia-wei, SONG Xiao-guo, CHEN Liang-bo, SUN Yi-zhan, LI Zhuo-lin. Ultrasound-assisted transient liquid phase bonding of AZ31B magnesium alloy using Al interlayer [J]. Materials Characterization, 2023, 196: 112556.

采用 Sn−2Al 钎料对 W90 钨合金进行超声辅助涂覆低温连接

宋晓国[1,2]，张旭东[1,2]，付 伟[1,2]，田晓羽[3]，吴广东[3]，胡胜鹏[1,2]

1. 哈尔滨工业大学 材料结构精密焊接与连接全国重点实验室，哈尔滨 150001；
2. 哈尔滨工业大学(威海) 山东特种焊接技术重点实验室，威海 264209；
3. 北京控制工程研究所，北京 100190

摘 要：采用 Sn−2Al 合金作为钎料，通过超声辅助涂覆技术，在 250 ℃、大气环境下对 W90 钨合金进行连接。研究了超声功率和超声时间对 Sn−2Al/W90 界面显微组织和界面强度的影响。超声波促进了 Sn−2Al 钎料在 W90 表面的润湿。随着超声功率的增加和超声时间的延长，焊缝中 Al 相的尺寸减小。Sn−2Al/W90 界面强度的最大值为 30.1 MPa。通过声压仿真和气泡动力学分析，发现空化效应的强度与超声功率成正比。空化效应产生的高温高压分别达到 83799.6 K 和 1.26×10^{14} Pa。

关键词：W−Ni−Fe 合金；Sn−Al 钎料；超声涂覆技术；声压；空化；气泡动力学

(Edited by Bing YANG)